Risk-Based Constraints for the Optimal Operation of an Energy Community

Dolanyi, Mihaly; Bruninx, Kenneth; Toubeau, Jean Francois; Delarue, Erik

DOI
10.1109/TSG.2022.3185310

Publication date
2022

Document Version
Final published version

Published in
IEEE Transactions on Smart Grid

Risk-Based Constraints for the Optimal Operation of an Energy Community

Mihaly Dolanyi, Kenneth Bruninx, *Member, IEEE*, Jean-François Toubeau, and Erik Delarue, *Member, IEEE*

***Abstract*—This paper formulates an energy community's centralized optimal bidding and scheduling problem as a time-series scenario-driven stochastic optimization model, building on real-life measurement data. In the presented model, a surrogate battery storage system with uncertain state-of-charge (SoC) bounds approximates the portfolio's aggregated flexibility. First, it is emphasized in a stylized analysis that risk-based energy constraints are highly beneficial (compared to chance-constraints) in coordinating distributed assets with unknown costs of constraint violation, as they limit both violation magnitude and probability. The presented research extends state-of-the-art models by implementing a worst-case conditional value at risk (WCVaR) based constraint for the storage SoC bounds. Then, an extensive numerical comparison is conducted to analyze the trade-off between out-of-sample violations and expected objective values, revealing that the proposed WCVaR based constraint shields significantly better against extreme out-of-sample outcomes than the conditional value at risk based equivalent. To bypass the non-trivial task of capturing the underlying time and asset-dependent uncertain processes, real-life measurement data is directly leveraged for both imbalance market uncertainty and load forecast errors. For this purpose, a shape-based clustering method is implemented to capture the input scenarios' temporal characteristics.**

***Index Terms*—Energy community, optimal bidding, stochastic optimization, risk-based constraints, temporal correlation.**

NOMENCLATURE

Parameters

$\Delta\widetilde{d}^{RT}_{t,\theta}$	Real-time forecast error at time t, in scenario θ
η^{ch}, η^{dch}	Charging and discharging efficiency (-)
λ^{DA}_t	Day-ahead energy market price at time t
$\widetilde{\lambda}^{RT}_{t,\theta}$	Real-time imbalance price at time t, scenario θ
$\overline{E}$	Energy capacity of the ESS (MWh)
$\overline{P}$	Power capacity of the ESS (MW)
$\underline{a}^{DA}$, $\overline{a}^{DA}$	Upper and lower limit of the community's day-ahead market position
$\underline{a}^{RT}$, $\overline{a}^{RT}$	Upper and lower limit of the community's real-time market position
d^{DA}_t	Day-ahead demand of the community at time t
$OPEX^{DA}$	Operational expenditure of the distributed storage.

Sets and indices

$\pi \in \Pi$	Load forecast error scenarios
$\theta \in \Theta$	Imbalance price scenarios
$d \in D$	Number of simulated days in the out-of-sample tests
$k \in K$	Clusters of load deviation scenarios
$n \in N$	Number of scenarios within cluster k
$t \in T$	Time steps.

Variables

$\Delta\widetilde{a}^{RT}_{t,\theta}$	Real-time imbalance bid of the community at time t, in scenario θ
$\Delta\widetilde{ch}^{RT}_{t,\theta,\pi}$, $\Delta\widetilde{dch}^{RT}_{t,\theta,\pi}$	Storage charging and discharging real-time deviations at time t, in scenario θ, π
a^{DA}_t	Day-ahead market bid of the community at time t
ch^{DA}_t, dch^{DA}_t	Charging and discharging of the storage scheduled in the day-ahead stage for time t
$SoC_{t,\theta,\pi}$	Storage state-of-charge at time t, in scenario θ, π.

I. Introduction

ENERGY communities (ECs) are envisioned to enhance the integration of distributed energy resources (DERs) into existing electricity markets, while incentivizing consumers and prosumers to unlock their flexibility potential [1]. In this paper, the joint coordination and market participation of several industrial sites, forming an EC, is modeled. The coordinating role is fulfilled by an energy community manager that performs a central optimization with partial knowledge of the coordinated asset's flexibility (leading to model uncertainty).

Manuscript received 16 November 2021; revised 5 April 2022; accepted 16 June 2022. Date of publication 22 June 2022; date of current version 21 October 2022. This work was supported in part by the Strategic Basic Research (SBO) under Grant S006718N provided by the Research Foundation—Flanders (FWO), and in part by the University of Leuven's C2 Research Project C24/16/018 entitled "Energy Storage as a Disruptive Technology in the Energy System of the Future." Paper no. TSG-01833-2021. *(Corresponding author: Mihaly Dolanyi.)*

Mihaly Dolanyi and Erik Delarue are with the Department of Mechanical Engineering, KU Leuven, 3000 Leuven, Belgium (e-mail: mihaly.dolanyi@kuleuven.be).

Kenneth Bruninx is with the Faculty of Technology, Policy and Management, TU Delft, 2628 CD Delft, The Netherlands, and also with the University of Leuven Energy Institute, TME Branch (Energy Conversion), Leuven, Belgium.

Jean-François Toubeau is with the Department of Power Electrical Engineering, Faculté Polytechnique de l'Université de Mons, 7000 Mons, Belgium.

Color versions of one or more figures in this article are available at https://doi.org/10.1109/TSG.2022.3185310.

Digital Object Identifier 10.1109/TSG.2022.3185310

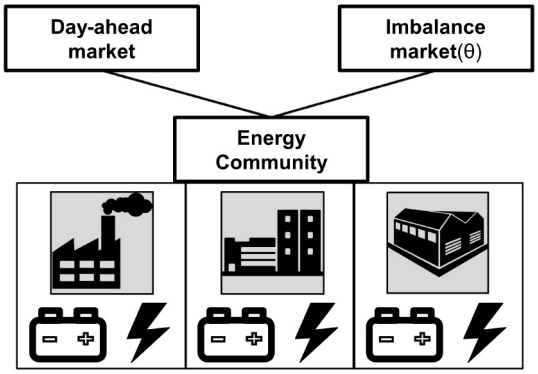

Fig. 1. Scheme showing the generic setting considered, involving multiple industrial sites with DERs. For the interaction with the markets two stages (DA, RT) are considered.

The EC faces both load forecast and market price uncertainty. Moreover, for some loads, the characterization of the forecast uncertainty may be highly ambiguous.[1] The different sites on-site flexibility can be represented as a battery storage system (BSS), complemented with a given inflexible residual load, reflecting the non-shiftable energy exchanges (Fig. 1), as done in, i.e., [2] for a set of thermostatically controlled loads. However, the state-of-charge (SoC) bounds of the approximating BSS model are subject to both parameter and model uncertainty. These uncertainties may be addressed by probabilistic constraints (most commonly by chance-constraints [3]) in stochastic optimization. Chance constraints (CCs) impose that the energy bounds are satisfied with a certain probability $\mathbb{P} \leq 1$, used, e.g., in [4], [5]. Assuming the several sources of multidimensional uncertainty ($\theta = \{1, \ldots, \Theta\}$, $\pi = \{1, \ldots, \Pi\}$), as used in the presented research, the CC formulation reads as $\mathbb{P}(g(x, \theta, \pi) \leq 0) \leq (1-\epsilon)\ \forall t$. Note that the probability is measured on both θ and π sets, but defined individually per time step t. CCs suffer from two drawbacks in the problem setting in this paper:

(1) This paper captures the underlying temporally correlated stochastic inputs via time-series scenarios. Chance constraints imposed on such correlated uncertainties typically only permit computationally expensive mixed-integer linear programming reformulations [6]. Authors of [7], [8] provide a tractable numerical approximation, but this approach may lead to undesired levels of conservativeness for multidimensional uncertainties, as considered in this paper.

(2) Conceptually CCs do not control the severity of the violation, allowing for infinitely large in-sample violations (discussed in Section III). The cost of violating the constraints of the considered assets, e.g., thermal comfort constraints, is usually unknown and time-varying. Hence, it may be highly beneficial to model energy bounds in a probabilistic framework that also imposes limitations on the violation magnitude.

Therefore, this paper builds on an alternative convex (conservative) approximation of CCs, which is called the conditional-value-at-risk based constraint (CVaR-BC) [9], employed, e.g., in [10]–[13]. This formulation allows for considering both the probability and the severity, which is in finance often used for constraining the maximum risk of a portfolio selection problem [14], [15]. Furthermore, CVaR is a coherent risk measure [16], and thus can be recast as a convex linear programming problem when the corresponding function is linearly dependent on the decision variables [11], even if correlated time-series scenarios are used as inputs.

Generating correlated (temporally or spatially) scenarios from the available data is a non-trivial task requiring appropriate understanding of the underlying uncertain process(es), which in addition, may differ per distributed asset in an energy community. Therefore, the scenario sampling used in this paper, is based on an advanced shape-based clustering technique [17] applied on the existing scenario samples. This technique provides an adequate distance measure to compare time-series samples, for which, the traditional Euclidean-distance may fail to capture important characteristics.

Both CC and the presented CVaR-BC suffer from the limitation that if the forecast error distribution of a newly accommodated site in the community differs significantly from the ones of the managed portfolio, i.e., the community manager faces distributional ambiguity, the resulting model is likely to exhibit poor out-of-sample performance. To overcome the issue of over-fitting the model to the limited information of the portfolio [18], distributionally robust optimization (DRO) provides performance guarantees [19], [20]. However, implementation of distributionally robust chance-constraints (DROCCs) [19], [21] in approximation algorithms like [7], [8] is non-trivial and may be computationally challenging.

To address the possible distributional ambiguity faced by the EC, a two-step modeling strategy is proposed. In the first step, building on the shape-based distance measure, the error scenarios are clustered into multiple groups, forming an exogenous ambiguity set. Next, based on this information, a worst-case CVaR [22], [23] based constraint (WCVaR-BC) is implemented to enforce the CVaR-BC in all scenario groups which may describe the true uncertainty. This modeling property offers higher out-of-sample reliability, when distributional ambiguity is present in the EC's portfolio. This paper utilizes the WCVaR' numerical advantage that it remains a convex and linear function, making it applicable for large scale power systems problems with temporally or spatially correlated uncertainty sets.

In the presented research, a large number of forecast error scenarios are already available via on-site measurements, serving as potential scenario candidates. Characterization of the ambiguity set, and thus providing inputs to the WCVaR model, for time series scenarios (instead of probability distributions) is not straightforward, and has not been addressed in state-of-the-art literature. To address this research gap a new modeling framework is developed, which connects the WCVaR-BC to a shape-based scenario clustering technique. Consequently, the distances between the scenario clusters may be used to define an ambiguity set (groups of scenarios) as the input of the WCVaR based models.

The main contributions of this paper are summarized as:

1) The proposed tractable probabilistic constraint extends the works of [10]–[13] by using the worst-case

[1]Distributional ambiguity is a concept for characterizing the limited knowledge about the exact underlying uncertainty, and is likely to faced by the EC when integrating new sites to the portfolio with limited historical measurements.

CVaR function to incorporate distributional ambiguity into correlated time-series scenario driven stochastic optimization.[2] The presented method is employed to enforce worst-case guarantees of the energy bound constraints (considering severity and frequency) within an energy community participating in both day-ahead and real-time energy markets.

2) A new modeling framework is developed, which connects the WCVaR-BC to a shape based clustering strategy. Therefore, an advanced shape-based clustering technique is implemented that better encapsulates temporal characteristics into the (dis)similarity measure among time-series scenarios, serving as inputs of the WCVaR-BC model.
3) First in a stylized example, the fundamental differences between CC and CVaR-BC, and then WCVaR-BC, are highlighted to motivate (i) the control of violation magnitudes, and (ii) the consideration of worst-case scenario sets. In the presented numerical studies the trade-off between violations and expected profits are extensively analyzed, illustrating that WCVaR-BC shields significantly better against extreme outcomes, while leading to only modest average cost increase. Furthermore, we show how the clustering strategy and observed distances among the clusters may relate to the performance of CVaR-BC and WCVaR-BC.

All developed models are published at https://github.com/Dmihaly/risky_community, to ease reproducibility and further developments. This paper continues as follows. In Section II the optimization problem of the EC and the clustering strategy is introduced. Then, in Section III, the CC, CVaR-BC, and WCVaR-BC are qualitatively compared against each other. Section IV introduces the details of the presented case studies and discusses both the results and their potential sensitivity w.r.t. the assumed in-sample scenario set. Lastly, Section V derives the conclusions and potential outlook.

II. Methodology

A. Model Formulation

In this Section, the centralized scheduling model for the energy community is introduced. It is assumed that the community has access to both day-ahead (DA) energy and real-time (RT) imbalance markets, as shown in Fig. 1. The exchange with the imbalance market is considered to be limited to avoid the virtual trading of large amounts of electricity. While such bidding strategy can be allowed (e.g., in the U.S.), or forbidden (e.g., in the EU), it may make more difficult to interpret the different constraint formulations. The scheduling is performed by a price-taking energy community manager [24]–[26], which is responsible to pool the loads and their flexibility potential, thus mitigating the overall shortfall risk of the portfolio. First, a scalable formulation is presented to hedge the risk of infeasible schedules, based on CVaR-based probabilistic constraint. The approach is then extended to the worst-case CVaR based constraint to handle large ambiguity (e.g., for new clients with limited history). The resulting decision model is formulated as a stochastic scenario-based optimization program.

In our models, the DA market is considered as deterministic, while the imbalance market's outcome is stochastic, represented via a reduced number of time-series scenarios of imbalance price profiles. While the DA market's uncertainty may also impact the EC's decision making, DA electricity prices are more predictable than the imbalance prices in the day-ahead stage. Therefore, capturing their uncertainty may have a less pronounced impact on the results than less predictable sources of uncertainty (e.g., the imbalance market price and the DERs' load profile). The imbalance market price scenarios are obtained by clustering historical outcomes of the Belgian imbalance market. Likewise, the forecast errors associated with the industrial sites' load profiles are characterized by time-series scenarios. In particular, the clients are represented using real measurements from several industrial and commercial sites (collected by Schneider Electric [27]), including energy consumption, local production and corresponding forecast errors. The main focus of this research is on how these forecast errors can be managed using risk-based constraints on the state-of-charge limits.

It is assumed that the community manager (CM) optimizes centrally all exchanges with the electricity markets and the scheduling of the individual DERs through their abstract ESS model. The collective day-ahead (*here-and-now*) and real-time (*recourse*) decisions $\mathcal{X}_{ec} = \{x_{ec}^{DA}, \widetilde{x}_{ec}^{RT}\}$ are the community's exchange with day-ahead and imbalance markets, and the individual decision variables inherit from the abstract flexibility model of each industrial site, i.e., DER agent $j \in \mathcal{J}$ on $\mathcal{X}_{der_j} = \{x_{der_j}^{DA}, \widetilde{x}_{der_j}^{RT}\}$. The collection of DER agents is represented as an aggregated asset (*der*). The cost components of the objective function are defined as:

$$C_m^{DA}\left(x_{ec}^{DA}\right) = \sum_{t\in\mathcal{T}} \lambda_t^{DA} \cdot a_t^{DA} \tag{1}$$

$$\widetilde{C}_m^{RT}\left(\widetilde{x}_{ec}^{RT}\right) = \sum_{t\in\mathcal{T}} \sum_{\theta\in\Theta} P_\theta \cdot \widetilde{\lambda}_{t,\theta}^{RT} \cdot \Delta\widetilde{a}_{t,\theta}^{RT} \tag{2}$$

$$C_{der}^{DA}\left(x_{ec}^{DA}, x_{der}^{DA}\right) = \sum_{t\in\mathcal{T}} OPEX^{DA} \cdot \left(dch_t^{DA} + ch_t^{DA}\right) \tag{3}$$

$$\widetilde{C}_{der}^{RT}\left(\widetilde{x}_{ec}^{RT}, \widetilde{x}_{der}^{RT}\right) = \sum_{t\in\mathcal{T}} \sum_{\theta\in\Theta} \sum_{\pi\in\Pi} P_\theta \cdot P_\pi \cdot OPEX^{RT} \cdot \left(\Delta\widetilde{dch}_{t,\theta,\pi}^{RT} + \Delta\widetilde{ch}_{t,\theta,\pi}^{RT}\right) \tag{4}$$

Eq. (1) and Eq. (2) denotes the sourcing cost of electricity from the DA energy market and the expected sourcing cost from the RT imbalance markets. The latter's uncertainty is captured via the scenario set θ. Eq. (3) describes the operational expenditure associated with the activation of the distributed BSS at the day ahead stage, while Eq. (4) defines the same expected cost at the second, real-time stage, whose uncertainty is captured by the set π. The central optimization problem of the energy

[2]Both CVaR and WCVaR may be used in the objective function of a given market participant to capture its risk-averse attitude [22], [23]. In this paper, we leverage these works to formulate probabilistic constraints as a set of linear functions.

community (EC) reads as:

$$\text{EC:} \min_{\mathcal{X}_{agg},\mathcal{X}_{der}} \quad \mathcal{F}_{EC} = C_m^{DA} + \widetilde{C}_m^{RT} + C_{der}^{DA} + \widetilde{C}_{der}^{RT} \tag{5a}$$

s.t.

$$\underline{a}^{DA} \le a_t^{DA} \le \overline{a}^{DA} \quad \forall t \tag{5b}$$

$$\underline{a}^{RT} \le \Delta\widetilde{a}_{t,\theta}^{RT} \le \overline{a}^{RT} \quad \forall t, \forall\theta \tag{5c}$$

$$a_t^{DA} + dch_t^{DA} - ch_t^{DA} - d_t^{DA} - \Delta\widetilde{d}_{t,\pi}^{RT} + \Delta\widetilde{a}_{t,\theta}^{RT} + \Delta\widetilde{dch}_{t,\theta,\pi}^{RT} - \Delta\widetilde{ch}_{t,\theta,\pi}^{RT} = 0 \quad \forall t, \forall\theta, \forall\pi \tag{5d}$$

$$0 \le dch_t^{DA} \le \overline{P} \quad \forall t \tag{5e}$$

$$0 \le ch_t^{DA} \le \overline{P} \quad \forall t \tag{5f}$$

$$0 \le \Delta\widetilde{dch}_{t,\theta,\pi}^{RT} \quad \forall t, \forall\theta, \forall\pi \tag{5g}$$

$$0 \le \Delta\widetilde{ch}_{t,\theta,\pi}^{RT} \quad \forall t, \forall\theta, \forall\pi \tag{5h}$$

$$dch_t^{DA} + \Delta dch_{t,\theta,\pi}^{RT} \le \overline{P} \quad \forall t, \forall\theta, \forall\pi \tag{5i}$$

$$ch_t^{DA} + \Delta ch_{t,\theta,\pi}^{RT} \le \overline{P} \quad \forall t, \forall\theta, \forall\pi \tag{5j}$$

$$SoC_{t,\theta,\pi} = SoC_{t-1,\theta,\pi} + \eta^{ch} \cdot \left(ch_t^{DA} + \Delta\widetilde{ch}_{t,\theta,\pi}^{RT}\right) - \left(dch_t^{DA} + \Delta\widetilde{dch}_{t,\theta,\pi}^{RT}\right)/\eta^{dch} \quad \forall t \setminus T, \forall\theta, \forall\pi \tag{5k}$$

$$SoC_{t,\theta,\pi} = SoC_{1,\theta,\pi} + \eta^{ch} \cdot \left(ch_t^{DA} + \Delta\widetilde{ch}_{t,\theta,\pi}^{RT}\right) - \left(dch_t^{DA} + \Delta\widetilde{dch}_{t,\theta,\pi}^{RT}\right)/\eta^{dch} \quad t = T, \forall\theta, \forall\pi \tag{5l}$$

$$0 \le SoC_{t,\theta,\pi} \le \overline{E} \quad \forall t, \forall\theta, \forall\pi \tag{5m}$$

Objective function (5a) is the concatenation of the individual cost components described by Eq. (1)-(4). Eq. (5b)-(5c) enforces that bids of the aggregator are within the predefined limits. This consideration reflects that in practice, the energy community is unlikely to perform virtual bidding with large amounts of electricity, i.e., its bids are limited by the capacity of the available assets. Eq. (5d) is the energy balance constraint of the community. Constraints (5e)-(5j) guarantee that both day-ahead and real-time charging and discharging decisions comply with the power bounds. Eq. (5k)-(5l) track the temporal evolution of the stored energy. Eq. (5k) characterizes the energy level evolution between time-step $t-1$ and t in the BSS, by adding the charged and subtracting the discharged energy (corrected with their corresponding efficiencies). Similarly, Eq. (5l) imposes the cyclic boundary condition on the state-of-charge. Lastly, constraint (5m) ensures that the stored energy is within the technical bounds. These bounds, however, may be highly uncertain and we therefore relax their strict enforcement in Section III. It is assumed that the exchanges of the individual sites does not lead to violations of any constraints of the distribution grid, hence, no power flow equations are modeled. If this would be the case, distribution grid constraints can be straightforwardly integrated in the presented framework, see, e.g., [28].

B. Clustering and Its Connection to the Model Formulation

The time-series scenarios, capturing the underlying uncertainty of the load were constructed by assembling empirical daily forecast errors from an extensive data set published by Schneider Electric (SE), containing historical electric load profiles of 70 anonymized industrial sites with the corresponding rolling-horizon forecasts, inspired by [29]. The data was collected mostly locations in Europe and in the United States. The data-set involves measurements from 2013 to 2017 (with 15 minutes resolution), but the availability of each site's measurements differ among the years. The most complete measurements are available in year 2016.

As several sites are included in the data set with different magnitudes of loads, the relative (to the day-ahead forecast) real-time load deviation, i.e., the relative forecast error, is calculated as:

$$\text{relative deviation} = \frac{d_t^{DA} - \Delta\widetilde{d}_{t,\pi}^{RT}}{d_t^{DA}} \tag{6}$$

The collection of these forecast errors serves as the input for the scenario-based stochastic optimization, and initialized by the following strategy:

1) The forecast error scenarios are ordered into K clusters based on their similarity/dissimilarity for each site $i \in I$.
2) Assuming each cluster $K = \{K_1, \ldots, K_N\}$ captures a particular trend of the uncertain process, i.e., different underlying distributions, N sequences are selected from each cluster, resulting in $\Pi = N \cdot |K|$ scenarios.

In the clustering step, we use a shape-based distance measure proposed in [17], and implemented in [30], to characterize the similarity/dissimilarity between time-series forecast error scenarios. Mentioned in [31], the employed shape-based clustering accounts for the temporal correlation in the data and is less sensitive to scale, noise and time-shifts. The dissimilarity measure used in the clustering may be also utilized to ex-ante control the distance between the K scenario clusters, leading to adjusted robustness in the optimization.

III. Qualitative Comparison of CC, CVaR-BC and WCVaR-BC

This Section provides insights into the fundamental differences and similarities between chance constrains (CCs), i.e., value-at-risk (VaR) based constraints, CVaR-BC, and the proposed WCVaR-BC. For this purpose we connect the VaR, CVaR and WCVaR functions through a stylized example, which illustrates how the different constraints penalize (or ignore) the magnitude of constraint violations.

Figure 2a depicts a hypothetical scenario set with their corresponding probability of occurrence. Assuming that the confidence level is set to 0.8 for the probabilistic constraint, violations may occur in 3 (indicated by orange) out of the 10 scenarios. The height of each column corresponds to the probability of the scenarios. Furthermore, Fig. 2b shows two alternative shapes at the violating scenarios via differentiated probabilities. Fig. 2 will be used in the following to describe the differences between VaR and CVaR.

To introduce the VaR and CVaR, a convex function $g(x, \omega)$ is used, where $x \in X$ are the set of decision variables, and $\omega \in \Omega$ composed of $\pi \in \Pi, \theta \in \Theta$ are the set of stochastic scenarios. The VaR for the upper (1-ϵ)-quantile of the joint bivariate distribution (Ω) is formulated as:

$$\overline{VaR}(\epsilon, x, \omega) = \inf_{\overline{\eta}}\{\overline{\eta} : \mathbb{P}(\omega | g(x, \omega) < \overline{\eta}) \le (1 - \epsilon)\} \tag{7a}$$

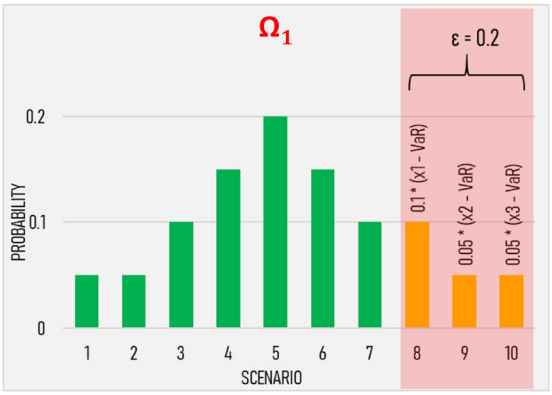

(a) Aggregated

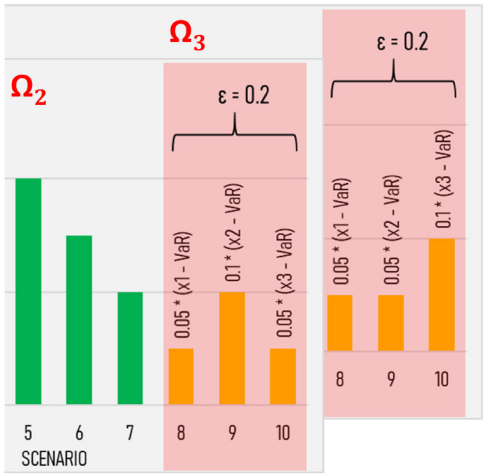

(b) Differentiated tails

Fig. 2. Green columns on the left-hand-side refer to the scenarios within the confidence interval characterized by $1-\epsilon$, i.e., no constraint violation allowed. In the orange scenarios violations are allowed. (a) VaR's and CVaR's positions are shown for comparison for a single distribution Ω_1 (b) indicates the changes for CVaR if different tails are considered in the alternative distributions Ω_2, Ω_3.

For lower (1-ϵ)-quantile, VaR reads as:

$$\underline{VaR}(\epsilon, x, \omega) = \sup_{\underline{\eta}} \left\{ \underline{\eta} : \mathbb{P}(\omega | g(x, \omega) < \underline{\eta}) \leq (1-\epsilon) \right\} \quad (7b)$$

where $\epsilon \in [0,1]$

$\overline{VaR}$ in Eq. (7a) is the largest value of η guaranteeing that the probability of having a function value greater than η is lower than or equal to (1 - ϵ). Constraining the VaR function as well as using CCs guarantees that in the green scenarios of Fig. 2, defined by an exogenous confidence level (1 - ϵ), no in-sample violation will occur. On the other hand, in the violating, orange scenarios, any level of violation is allowed by this formulation. Note that the three different distributions ($\Omega_1, \Omega_2, \Omega_3$) are identical through the lens of the VaR function, i.e., CCs or VaR-based constraints are indifferent w.r.t. shape of the tail.

Contrary to Eq. (7a) and Eq. (7b), the CVaR characterizes the mean function value of the instances exceeding the VaR, i.e., the expected value of the scenarios at the tail (orange scenarios). Incorporating the degree of violation of scenarios and their corresponding probabilities, may lead to more restrictive outcomes compered to CCs. Therefore, CVaR-BC may be seen a convex approximation of the CC [32].

Following the formulation developed in [9], [33], the upper and lower CVaR functions are defined as:

$$\overline{CVaR}(\epsilon, x, \omega) = \inf_{\overline{\eta}} \left\{ \overline{\eta} + \frac{1}{1-\epsilon} \mathbb{E}\left[g(x, \omega) - \overline{\eta} \right]^+ : \overline{\eta} \in \mathbb{R} \right\} \quad (7c)$$

$$\underline{CVaR}(\epsilon, x, \omega) = \sup_{\underline{\eta}} \left\{ \underline{\eta} - \frac{1}{1-\epsilon} \mathbb{E}\left[\underline{\eta} - g(x, \omega) \right]^+ : \underline{\eta} \in \mathbb{R} \right\} \quad (7d)$$

where $[t]^+ = max(t, 0)$. Elimination of the plus function, as in [33], leads to the following linear programming forms:

$$\overline{CVaR}^*(\epsilon, x, \omega) = \overline{\eta} + \frac{1}{1-\epsilon} \mathbb{E}\{\delta(\omega) : \delta(\omega) \geq (g(x, \omega) - \overline{\eta})\} \quad (7e)$$

$$\underline{CVaR}^*(\epsilon, x, \omega) = \underline{\eta} - \frac{1}{1-\epsilon} \mathbb{E}\left\{ \delta(\omega) : \delta(\omega) \geq (\underline{\eta} - g(x, \omega)) \right\} \quad (7f)$$

where $\delta \in \mathbb{R}^+$ is an auxiliary variable. The above reformulation leads to significant computational advantages when modeling CVaR, compared to VaR or CC, making it easily suitable for multi-source time-series scenario inputs in large-scale stochastic problems. Using the above functions, we recast the energy content constraints Eq. (5m) of the BSS as upper or lower conditional-value-at-risk constraints.

$$SoC(x, \omega) \leq \overline{E} \Leftrightarrow \overline{CVaR}^*_{SoC}(\epsilon, x, \omega) \leq \overline{E} \quad (7g)$$

$$SoC(x, \omega) \geq 0 \Leftrightarrow \underline{CVaR}^*_{SoC}(\epsilon, x, \omega) \geq 0 \quad (7h)$$

The fact that CVaR-BC can be modeled by a convex function, implies that it results in continuously increasing/decreasing, monotone in-sample expected violations. In contrast, VaR (and CC) typically exhibit discrete jumps w.r.t. the confidence level. Such jumps may translate into inconsistent out-of-sample performance and expected outcomes can be significantly sensitive to the chosen confidence level. The above characteristics of the CVaR function make it particularly beneficial over CC in problems where violation costs are hard to be characterized ex-ante, e.g., for thermal discomfort [34].

In Table I, the different expected violations are calculated, resulting from the alternative tails of Fig. 2a and Fig. 2b. The assumed violations for Scenarios {8, 9, 10} are {1.0, 1.5, 2.0}. It can be noted that in the three different cases the modeler accepts very different levels of expected violations, despite the fixed violation level, which is ignored in the formulation of CCs. On the other hand, in the CVaR-BC this property is well-captured and can be compensated, e.g., by choosing lower violation levels in the more probable scenarios. A more methodological comparison of the CC (or VaR) and CVaR-BC may be found in [14], [35].

Opposed to the CVaR case, in which $\Omega_1, \Omega_2, \Omega_3$ belong to the same scenario cluster ($k = 1$), the worst-case CVaR (WCVaR) function is used to allow for differentiation among a collection of scenario clusters (Ω^k, $k \in \mathcal{K}$), e.g., $k = 1, 2, 3$ clusters can be characterized for $\Omega_1, \Omega_2, \Omega_3$. As a result,

TABLE I
EXPECTED AND AVERAGE VIOLATION IN THE VIOLATING SCENARIOS (AT THE TAIL OF THE DISTRIBUTIONS), I.E., CVAR, FOR THE THREE DIFFERENT DISTRIBUTIONS. THE EXPECTED VIOLATION IS CALCULATED BY THE PRODUCT OF THE ABSOLUTE VIOLATION AND THE CORRESPONDING SCENARIO'S PROBABILITY. THE VIOLATIONS FOR SCENARIOS {8,9,10} ARE {1.0,1.5,2.0}. THE FIRST NUMBER REFERS TO THE PROBABILITY OF THE VIOLATING SCENARIO (SEE FIG. 2)

	Distributions		
	Ω_1	Ω_2	Ω_3
Scenario 8	0.1*1.0	0.05*1.0	0.05*1.0
Scenario 9	0.05*1.5	0.1*1.5	0.05*1.5
Scenario 10	0.05*2.0	0.05*2.0	0.1*2.0
CVaR per tail	0.275	0.3	0.325
Avg. CVaR	0.3		

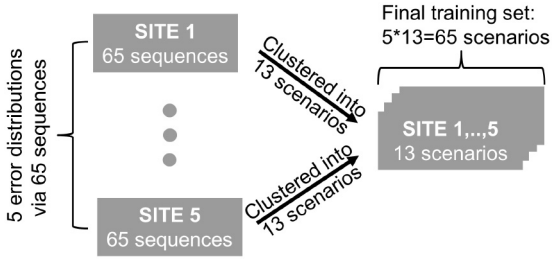

Fig. 3. Clustering strategy to define the in-sample scenarios. On the left, the collected error sequences for each 5 site is indicated. Via reducing each 5 site's 65 sequences to 13 clusters, we attain $5 \cdot 13$ overall in-sample scenarios.

instead of aggregating the three tail approximations, the probabilistic constraint enforcement can be done for the worst one (Ω_3 in the stylized example, as shown in Table I). This way one can avoid over-fitting the model to the aggregation of all tails and reduce possible exposure to extreme outcomes. For a collection of scenario sets (Ω^k, $k \in K$), the WCVaR function is defined as the CVaR belonging to the worst realization:

$$\overline{WCVaR}(\epsilon, x, \omega) \triangleq \sup_{k \in K} \overline{CVaR}^k\left(\epsilon, x, \omega^k\right) \tag{7i}$$

$$\underline{WCVaR}(\epsilon, x, \omega) \triangleq \inf_{k \in K} \underline{CVaR}^k\left(\epsilon, x, \omega^k\right) \tag{7j}$$

It is shown in [22] that WCVaR remains a coherent risk measure. Furthermore, the same linear approximation may be used for WCVaR, as derived for CVaR in [9], under the assumption that $f(x, \omega)$ is linear w.r.t. x, and X is a convex polyhedron. Consequently the resulting SoC constraints may be written as a worst-case constraint that holds for all CVaR-s, belonging to set K:

$$\overline{CVaR}^k_{SoC} \leq \overline{WCVaR}_{SoC} \leq \overline{E} \quad \forall k \in K \tag{7k}$$

$$\underline{CVaR}^k_{SoC} \geq \underline{WCVaR}_{SoC} \geq 0 \quad \forall k \in K \tag{7l}$$

In the model formulation, CVaR is defined over the set of scenario clusters K, as defined in Section II-B, allowing for differentiation in its values. Then the worst-case CVaR (WCVaR) function [22], [23] is used to endogenously account for the worst realization of CVaR. Note, that when the model is supplied by a single cluster of scenarios ($k = 1$), CVaR and WCVaR are identical.

IV. NUMERICAL RESULTS

In this section, we evaluate the performance of our proposed WCVaR constraints w.r.t. CVaR-BC in modeling the energy bounds of the flexibility providers. In particular, the model is tested on an energy community composed of 5 industrial loads (denoted as MIX), referred to as {19, 35, 40, 58, 62}, randomly selected from the Schneider Electric dataset [27]. First, the clustering technique, described in Section II-B, is applied to construct the representative load error scenarios. We make the assumption that each of the 5 sites are characterized by a different underlying assumption on the distribution Ω^k, where $k = 1, 2, 3, 4, 5$. For each site, the distribution is modelled through sequences that are collected from all weekdays in the time-horizon of three months, from January to March in 2016, which results in 65 sequences for each site. These sequences are clustered into 13 clusters for each site. In each cluster, the closest element (defined by using the shape-based distance function [17]) to the centroid is selected as a prototype. The assigned probability of occurrence is proportional to the size of the cluster from which the prototype is selected. Lastly, each cluster's prototype and its probability of occurrence is moved to the final set of in-sample scenarios, leading to overall 65 scenarios (13 representative sequences for the 5 industrial clients). When using CVaR-BC no differentiation is made based on which site was the root of a given scenario, whereas this information is preserved in WCVaR to make distinction among the $k \in K$ scenario clusters, i.e., $k \in K$ underlying distributions.

Below, we first introduce the data used in the numerical case studies. Then, in Section IV-A, we compare the out-of-sample reliability (obtained by CVaR-BC and WCVaR-BC). Lastly, we highlight the mean as well as the maximum violations in function of the corresponding objective value (Section IV-B).

In the case studies, we assume that the only varying (uncertain) parameters are the real-time load realizations (forecast error with respect to day-ahead expectations), whereas the day-ahead forecasted load is used from a single day to focus the analysis on the effects of uncertainty. Furthermore, for the sake of simplicity, we model a single site assuming that it represents the aggregation of several DERs both in terms of fixed load and flexibility.[3] The modeled BSS, which acts as a surrogate for the flexible part of the load, has 3 MW of charging and discharging power (with 98% round-trip efficiency) and 0.4 MWh energy capacity. The daily price profiles were downloaded from ELIA's [36] (the Belgian Transmission System Operator) website. The DA market price is deterministic, and its average value over the day is $\bar{\lambda}^{DA}_t = 18.2$ €/MWh. and the expected average RT imbalance market price is $\mathbb{E}(\widetilde{\lambda}^{RT}_{t,\theta}) = 18.6$ €/MWh. To model the uncertainty of real-time electricity prices, 5 scenarios are considered in the optimization, obtained by clustering the yearly data into the 5 representative clusters and selecting their prototypes. Similarly to the DA forecasted part of the demand, the deterministic DA market price and the stochastic RT market price scenarios ($\theta \in \Theta$) are not altered in the simulations. To avoid unrealistic exchanged quantities

[3]This is solely a modeling simplification and the framework would allow for the inclusion of multiple sites.

with the markets, and extensive virtual bidding, the DA market position of the community is limited to two times the maximal forecasted load (Eq. (5b)), whereas the RT market position is bounded by half of the maximal load deviation (Eq. (5c)) in all considered scenarios. The operational expenditure (OPEX) of the DER's flexibility is $0.01 \cdot \bar{\lambda}_t^{DA}$ in the DA stage and $0.05 \cdot \mathbb{E}(\widetilde{\lambda}_{t,\theta}^{RT})$ in the RT recourse stage in €/MWh. The higher RT OPEX intends to reflect the increasing communication and scheduling burden when executing deviations closer to real-time.

In the in-sample optimization, the stochastic model is supplied with all the input data such as the DA and RT market prices (with 5 scenarios), the deterministic (fixed) DA forecasted load profile and the generated RT forecast error scenarios (65 scenarios). The 65 forecast error scenarios are constructed by applying the clustering technique (as presented in Section II-B) on the in-sample set of sites: {19, 35, 40, 58, 62}. Once optimality is reached, all DA decisions and the RT imbalance market positions are fixed in the optimization model used in the test runs. In the test runs the RT forecast error realization is being updated, which is the only altered input. Out-of-sample feasibility is not guaranteed due to the (i) in-sample violations of the probabilistic SoC constraints (Eq. 5m), (ii) the DA decisions and the RT imbalance market positions are fixed to the training model's outcome, i.e., only RT charging and discharging decisions are re-optimized, while the load forecast error takes different values. If the resulting imbalance exceeds the limit that the EC can trade with the RT imbalance market, the SoC bound constraints are assumed to be violated. To ensure that the model is out-of-sample feasible, an ancillary slack variable (s^{UP}, s^{DOWN}) is added to the SoC bounds (Eq. 5m). The non-zero values of the slack variables are penalized in the objective function with a large violation coefficient (1000 €/MWh), leading to the following extension of the objective function: $\sum_{t,d} \text{penalty} \cdot (s_{t,d}^{UP} + s_{t,d}^{DOWN})$. The penalty cost is not accounted for in the reported objective values. In summary, any imbalance in the EC's out-of-sample scheduling may be compensated by: (i) adjusting the imbalance market position until the corresponding constraints, Eq. (5c), allow for it (translating to financial losses), (ii) violating the SoC constraints via the related slack variables. The aim of the following case studies is to compare out-of-sample violation magnitudes (contrasted to the corresponding attained profits) faced by the EC when relying on the different probabilistic constraints.

Test simulations are conducted on 7 new sites {12, 58, 40, 17, 70, 68, 29}, which were not part of the training set. For each site, 65 days are simulated per confidence level, leading to 65 out-of-sample scenarios for each 10 confidence levels. The updated parameter is the daily forecast error, i.e., the uncertain part of the demand which was also collected from the Schneider Electric dataset from January 2016 to March 2016.

A. In- and Out-of-Sample Reliability Comparison of CVaR-BC and WCVaR-BC

Fig. 4 depicts the out-of-sample reliability as a function of the in-sample confidence level. The reliability is calculated

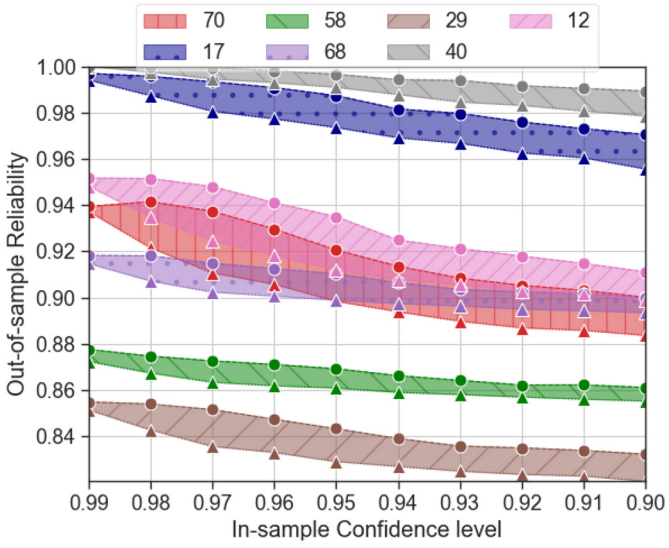

Fig. 4. The reliability (-), calculated based on the number of violating instances in the test runs attained under the given in-sample confidence levels (%). Triangle markers indicate the results of the CVaR-BC and circles the outcomes resulted from the WCVaR-BC. The numbers in the legend refer to the test site's id.

based on the total number of violating instances, i.e., cases in which $s_{t,d}^{UP}, s_{t,d}^{DOWN}$ are non-zero were enumerated in all time steps ($t \in T$) and in all simulated days ($d \in D$), and the total optimized time-steps, i.e., number of time steps multiplied by the number of days. The results indicate that WCVaR-BC (indicated by circle markers) leads to always higher reliability than CVaR-BC (triangle markers) for all subject sites. Although, the difference is more pronounced for some sites (e.g., for 70, 12), WCVaR's higher reliability is an expected outcome given the more conservative nature of the WCVaR function.

A factor of crucial importance influencing the out-of-sample performance is the difference between the inputs used in the out-of-sample simulations and the inputs used in the training (in-sample) phase of the optimization. Obviously one can expect better performance if the in-sample uncertainty approximation is closer to the realized inputs. When selecting the test sites, it was taken into consideration that the test set should involve various samples w.r.t. their closeness to the in-sample data. To characterize the (dis)similarity between in-sample and out-of-sample instances, the same shape-based distance was used as in the clustering step for scenario reduction. In Fig. 5 it is shown how the average[4] sequence of a few selected test site compares to the average sequence of the in-sample training MIX. It is visible that site 12 is the most similar whereas 29 has the highest dissimilarity. The quantified distances between the prototype of each test site and the training set are summarized in Table I, confirming that site 12 is indeed the closest match, whereas site 29 is one of the highest dissimilarity. The possible correlation of these distances to the changes in

[4]The average instance is calculated by using the shape extraction function of the shape-based clustering method.

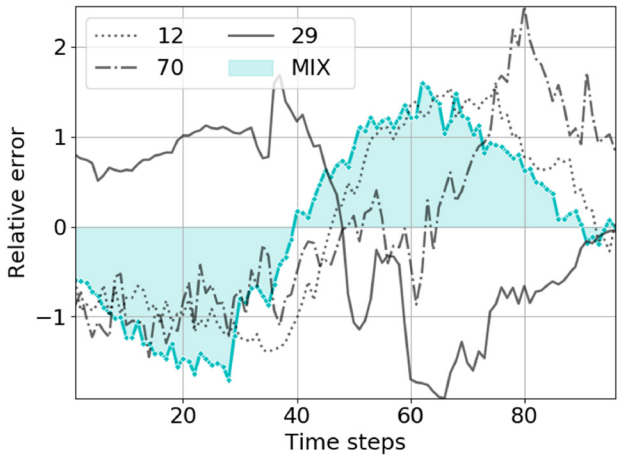

Fig. 5. The extracted prototypes using the shape extraction function of [30]. *MIX* indicates the prototype of the in-sample training set, whereas 12,29,70 refer to the prototype of three test sites.

the out-of-sample performance, e.g., in the number of violations for the probabilistic constraints are discussed later in this section.

B. The Trade-Off Between Violations and Expected Profits

In Fig. 6, in the left y-axis the mean daily operation cost is plotted, calculated by the following function: $\frac{1}{N_d} \cdot \sum_{t,d} \mathcal{F}_{t,d}^{EC}$, where N_d refers to the number of simulated days for each confidence level. Note that the EC makes a profit in its daily operation. However, here the negative costs are plotted to better visualize their comparison with the mean daily violations: $\frac{1}{N_d} \cdot \sum_{t,d} (s_{t,d}^{UP} + s_{t,d}^{DOWN})$, shown on the right y-axis.

The WCVaR-BC by definition imposes more conservative constraints such that the higher reliability comes at the cost of lower expected mean performance. This can be understood by looking at the projections in Fig. 6. If, e.g., one compares the cost obtained by WCVaR-BC at $\epsilon = 0.08$, for site 12 a similar cost can be obtained at $\epsilon = 0.03$ by CVaR-BC. The mean violations, however, differ significantly at the chosen confidence levels, despite that costs are close to each other. The difference is showing that WCVaR-BC may lead to higher average violation when calibrated to achieve similar objective values as CVaR-BC (indicated by the red Δ sign). The same projections, made for site 29, show a significantly smaller difference, which may be explained by the different distances from the training scenario MIX. It is also visible that in lower confidence levels, the operational costs are converging, whereas the corresponding violations remain lower with WCVaR-BC.

The results of Fig. 6 suggests that CVaR-BC on average leads to higher reliability for a given average out-of-sample cost. However, as discussed in the motivation of WCVaR-BC, its advantage lies in the ability to reduce the exposure to extreme out-of-sample outcomes, which has the most added value when limited historical information is available to approximate the uncertain process.

The extreme outcomes, i.e., instances with the highest out-of-sample violations due to the wrong approximation of the underlying uncertainty, are not well depicted in the aggregated results of Fig. 4 and Fig. 6. Therefore, it is insightful to assess the spread of the maximum violations as a function of the corresponding profit in each violating case (Fig. 7).

TABLE II
THE DISTANCE BETWEEN EACH SITE'S PROTOTYPE AND THE MEAN SEQUENCE OF THE IN-SAMPLE SCENARIO MIX, CALCULATED BASED ON THE SHAPE-BASED DISTANCE

Site	12	58	40	17	70	68	29
Distance	0.055	0.159	0.258	0.294	0.268	0.510	0.501

Figure 7 shows the bi-variate kernel density estimate (KDE) plot indicating the expected spectrum of the maximum observed daily violations and the corresponding profits for sites {12, 70, 29}. In addition, on the marginal x and y axis the histograms are plotted individually for the distribution of both maximum violations and profits. WCVaR-BC leads to lower violations and lower profits by definition. However, it was observed in the analysis that reducing the confidence level by 5-7 percentage points often leads to similar expected profits by WCVaR-BC as by CVaR-BC. Therefore, to generate results from the same frontier in the comparison of maximum violations, the WCVaR-BC model was solved to lower confidence levels ($\epsilon = 0.01 - 0.17$, meaning 83% was the lowest confidence). The maximum violations are collected for each 65 real-time forecast error realizations and for each in-sample confidence level (#10, #17). Overall this leads to 650 possible violations with CVaR-BC and to 1105 with WCVaR-BC. Due to the difference in the number of studied instances, we normalized both the histograms and the KDE plots, such that their area always adds up to one.

Fig. 7a shows that the advantage of using WCVaR-BC is the most prominent for site 29, which is the second furthest candidate from the in-sample scenario MIX (Table II). It can be observed that the maximum violations reach a more than two times higher level than for site 12 and 70 at the tail of the distribution (Fig. 7a marginal y-axis), while the profits are spread mostly in the same range (Fig. 7a marginal x-axis). For this site, the in-sample scenario set was a particularly inaccurate approximation, as such the severity of the maximum violating instances are large with CVaR-BC that fits the model tighter to the training set. WCVaR-BC, on the contrary, was capable to circumvent such severe violations, remaining in the same range as for the other two sites (shown by the marginal y-axes of Fig. 7). Contrary to site 29, the outcomes of site 12 (Fig. 7b), the best match with the training set, indicate moderately lower maximum violations with CVaR-BC compared to WCVaR-BC. Site 70, which is representative for most other test sites not shown in the Fig. 7, does not show pronounced differences in using CVaR-BC or WCVaR-BC. The profits as well as the maximum violations are similarly distributed. The three different sites shown by Fig. 7 demonstrate well the trade-off faced by the modeler when choosing between the two proposed risk-based constraints.

C. The Impact of Using Alternative Training Sets

As highlighted in Section IV-B the WCVaR-BC's most significant advantage over CVaR-BC is its property to limit

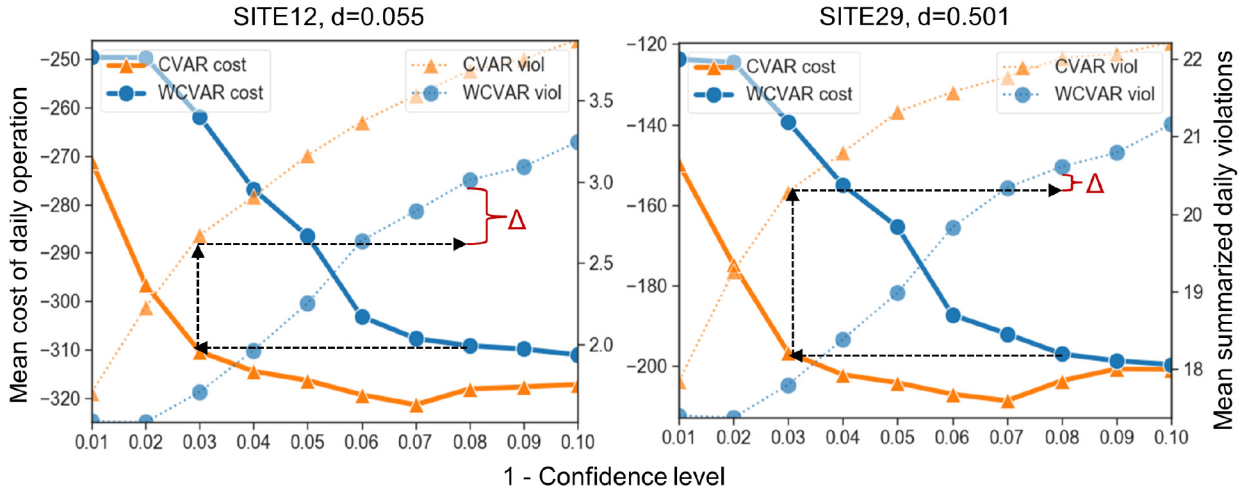

Fig. 6. Mean out-of-sample cost of daily operation in €(left-hand-side of the y-axis) and mean daily upper plus lower bound violations (MWh) of the SoC constraint (right-hand-side of the y-axis) is plotted in function of the confidence level $(1-\epsilon)$. The black dashed rectangle indicates an example of comparing WCVaR-BC$^{92\%}$ to CVaR-BC$^{97\%}$ in terms of daily operational cost and the mean daily violations. The red Δ sign highlights that the WCVaR-BC violation is higher corresponding to around the same operational cost as attained by CVaR-BC. The "d" letter on the top of each figure indicate the difference between the prototype of the in-sample mix and the test site.

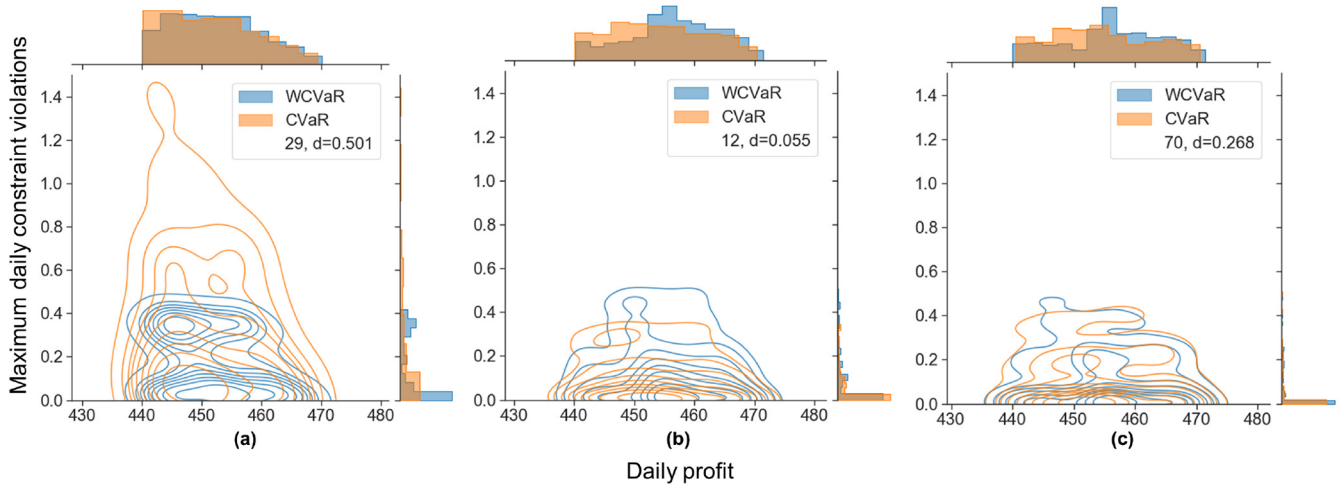

Fig. 7. In the center the kernel density estimation of the maximum daily violations (in MWh) and corresponding profits (in €) is shown, collected by solving CVaR-BC at $\epsilon = 0.01 - 0.1$ and WCVaR-BC at $\epsilon = 0.01 - 0.17$. In the marginal x and y axis the histograms for maximum violations and profits are plotted individually. From all the obtained results, we report the ones with the highest profit as they produce the highest violating instances. Therefore, the results were cut-off at the profit of €440 for all sites. All plots are normalized such that their area individually adds up to one.

extreme violations. The uncertainty captured via the training scenarios has essential influence on the performance of the discussed constraints. Selecting and evaluating this set is not straightforward, as numerous combinations exist and it is not known which one materializes in reality for the EC. Therefore, this section evaluates the sensitivity of the conclusions derived in Section IV-B w.r.t. changes in the training set. The altered scenario set involves {6,17,40,58,68} sites. The test sites, on the other hand, are not altered. The mean shape-based distance (SBD) between the test sites and the training set's prototype is now increased to 0.384, compared to the original's set's 0.292. This indicates significant reduction in the similarity between the training and test sets.

The tendency towards extreme violation is expressed by the 95th percentiles of daily constraint violation, mimicking the visual representation of Figure 7. Table III summarizes the changes (when using WCVaR-BC instead of CVaR-BC) in the 95th percentile constraint violations and in the corresponding mean daily profits. To obtain a fair comparison between the CVaR-BC and WCVaR-BC, a search method is implemented that mimics the projection made in Figure 6. First, the confidence level of the chosen CVaR-BC results is fixed to $\epsilon = 0.04$. Then, the ϵ in WCVaR-BC's set of results is selected which best matches the mean daily profit of the CVaR-BC result. The resulting profit differences (also indicated in Table III) never exceed 1%, mostly staying below 0%.

From the results it is visible that the extreme violation mitigating effect of the WCVaR-BC remains apparent for the new training set. The most significant reduction, however, occurs for a different site (68 instead of 29). Although the gain in the extreme high violations is less pronounced (0.17 MWh instead of 0.49 MWh) for the new scenario set, it remains significant.

TABLE III
THE CHANGES IN THE 95TH PERCENTILE OF DAILY CONSTRAINT VIOLATIONS (ΔVIOL) AND IN THE CORRESPONDING MEAN DAILY PROFITS (ΔPROFIT) BETWEEN THE RESULTS OF WCVAR-BC AND CVAR-BC FOR THE ORIGINAL TRAINING SET ($.^1$) AND THE ADJUSTED ONE ($.^2$). THE RESULTS FROM THE CVAR-BC MODEL ARE CHOSEN AT THE $\epsilon = 0.04$ CONFIDENCE LEVEL. THE CONFIDENCE LEVEL OF THE CORRESPONDING WCVAR-BC MODEL (INDICATED BY ϵ *WCVaR*) IS CHOSEN TO BEST MATCH THE CVAR RESULTS IN THE MEAN DAILY PROFIT. NEGATIVE VALUES REFER TO LOWER VIOLATIONS BUT ALSO LOWER PROFITS IN THE WCVAR CASE

Site	68	70	12	58	40	17	29
ΔViol^1 (MWh)	0	0.02	0.1	0.04	0.01	0	-0.49
ΔProfit^1 (%)	0	0	-1	0	0	0	-1
ϵ WCVaR	0.08	0.14	0.17	0.08	0.13	0.08	0.1
ΔViol^2 (MWh)	-0.17	0.03	-0.01	0.02	0.03	0.02	0.01
ΔProfit^2 (%)	0	0	-1	0	0	0	-1
ϵ WCVaR	0.1	0.13	0.17	0.11	0.12	0.11	0.12

It should be also noted that the 95th percentile of the violations for most sites stays in the same range in case of both in-sample scenarios sets.

V. CONCLUSION AND OUTLOOK

This paper implements two data-driven risk-based constraints for the risk-aware probabilistic enforcement of the flexibility bounds of an energy community that aggregates a variety of distributed assets, and participates in day-ahead energy and imbalance markets. First, the CVaR-BC is formulated to account for both the severity and the probability of the violations when representing the energy bounds of the EC, which carry potential gains over CCs. Next, the former constraint is extended to a novel WCVaR-BC that differentiates the CVaR value among the sub-clusters of clients, allowing to hedge against distributional ambiguity (inheriting from the varying nature of the on-site DER assets). The resulting time-series scenario-driven optimization models allow tackling large-scale problem instances in a linear programming fashion.

After qualitatively comparing the proposed constraints to CC, in a numerical analysis it was shown that WCVaR-BC allows for reducing the exposure to extreme violation levels, when assuming limited knowledge about the forecast errors. The proposed constraints can facilitate the flawless expansion of the EC's portfolio by assets with scarce historical data. Furthermore, the authors believe that the implemented modeling strategy may be well-suited for a broad range of power systems applications with ambiguous uncertainty sets and limited knowledge on the cost of constraint violations. The convex nature of the risk-based constraints allow for interpreting the associated dual variables as prices in local energy markets. In future research, this property may facilitate the risk-aware trading of flexible resources.

As future research, the impact of clustering can be further investigated, in the interest of better understand how the number of scenarios and the distance among them can influence the out-of-sample performance of the risk-based constraints.

ACKNOWLEDGMENT

The authors would like to thank for the insightful comments of Geert Deconinck and Adriano Arrigo in the process of shaping the presented research. K. Bruninx is a post-doctoral research fellow of the Research Foundation - Flanders (FWO) at the University of Leuven and EnergyVille (mandate no. 12J3320N).

REFERENCES

[1] T. Morstyn, N. Farrell, S. J. Darby, and M. D. McCulloch, "Using peer-to-peer energy-trading platforms to incentivize prosumers to form federated power plants," *Nat. Energy*, vol. 3, no. 2, pp. 94–101, 2018.
[2] H. Hao, B. M. Sanandaji, K. Poolla, and T. L. Vincent, "Aggregate flexibility of thermostatically controlled loads," *IEEE Trans. Power Syst.*, vol. 30, no. 1, pp. 189–198, Jan. 2015.
[3] A. Charnes and W. W. Cooper, "Chance-constrained programming," *Manag. Sci.*, vol. 6, no. 1, pp. 73–79, 1959.
[4] H. Zhang, Z. Hu, E. Munsing, S. J. Moura, and Y. Song, "Data-driven chance-constrained regulation capacity offering for distributed energy resources," *IEEE Trans. Smart Grid*, vol. 10, no. 3, pp. 2713–2725, May 2019.
[5] J.-F. Toubeau, J. Bottieau, Z. De Greve, F. Vallee, and K. Bruninx, "Data-driven scheduling of energy storage in day-ahead energy and reserve markets with probabilistic guarantees on real-time delivery," *IEEE Trans. Power Syst.*, vol. 36, no. 4, pp. 2815–2828, Jul. 2021.
[6] S. Ahmed and D. J. Papageorgiou, "Probabilistic set covering with correlations," *Oper. Res.*, vol. 61, no. 2, pp. 438–452, 2013.
[7] K. Margellos, P. Goulart, and J. Lygeros, "On the road between robust optimization and the scenario approach for chance constrained optimization problems," *IEEE Trans. Autom. Control*, vol. 59, no. 8, pp. 2258–2263, Aug. 2014.
[8] M. Vrakopoulou, B. Li, and J. L. Mathieu, "Chance constrained reserve scheduling using uncertain controllable loads part I: Formulation and scenario-based analysis," *IEEE Trans. Smart Grid*, vol. 10, no. 2, pp. 1608–1617, Mar. 2019.
[9] R. T. Rockafellar and S. Uryasev, "Optimization of conditional value-at-risk," *J. Risk*, vol. 2, no. 3, pp. 21–42, 2000.
[10] Q. P. Zheng and P. M. Pardalos, "Stochastic and risk management models and solution algorithm for natural gas transmission network expansion and LNG terminal location planning," *J. Optim. Theory Appl.*, vol. 147, no. 2, pp. 337–357, 2010.
[11] Y. Huang, Q. P. Zheng, and J. Wang, "Two-stage stochastic unit commitment model including non-generation resources with conditional value-at-risk constraints," *Elect. Power Syst. Res.*, vol. 116, pp. 427–438, Nov. 2014.
[12] A. N. Madavan and S. Bose, "Risk-sensitive energy procurement with uncertain wind," in *Proc. 7th IEEE Global Conf. Signal Inf. Process. (GlobalSIP)*, 2019, pp. 896–920.
[13] T. Summers, J. Warrington, M. Morari, and J. Lygeros, "Stochastic optimal power flow based on conditional value at risk and distributional robustness," *Int. J. Elect. Power Energy Syst.*, vol. 72, pp. 116–125, Nov. 2015.
[14] G. J. Alexander and A. M. Baptista, "A comparison of VaR and CVaR constraints on portfolio selection with the mean-variance model," *Manag. Sci.*, vol. 50, no. 9, pp. 1261–1273, 2004.
[15] P. Krokhmal, J. Palmquist, and S. Uryasev, "Portfolio optimization with conditional value-at-risk objective and constraints," *J. Risk*, vol. 4, no. 2, pp. 43–68, 2002.
[16] F. Delbaen, "Coherent risk measures," *Blätter der DGVFM*, vol. 24, no. 4, pp. 733–739, 2000.
[17] J. Paparrizos and L. Gravano, "*k*-shape: Efficient and accurate clustering of time series," in *Proc. ACM SIGMOD Int. Conf. Manag. Data*, 2015, pp. 1855–1870.
[18] H. Yang *et al.*, "Distributionally robust optimal bidding of controllable load aggregators in the electricity market," *IEEE Trans. Power Syst.*, vol. 33, no. 1, pp. 1089–1091, Jan. 2018.
[19] S. Zymler, D. Kuhn, and B. Rustem, "Distributionally robust joint chance constraints with second-order moment information," *Math. Program.*, vol. 137, nos. 1–2, pp. 167–198, 2013.
[20] P. M. Esfahani and D. Kuhn, "Data-driven distributionally robust optimization using the Wasserstein metric: Performance guarantees and tractable reformulations," *Math. Program.*, vol. 171, nos. 1–2, pp. 115–166, 2018.

[21] A. Arrigo, C. Ordoudis, J. Kazempour, Z. De Grève, J.-F. Toubeau, and F. Vallée, "Wasserstein distributionally robust chance-constrained optimization for energy and reserve dispatch: An exact and physically-bounded formulation," *Eur. J. Oper. Res.*, vol. 296, no. 1, pp. 304–322, 2022.
[22] S. Zhu and M. Fukushima, "Worst-case conditional value-at-risk with application to robust portfolio management," *Oper. Res.*, vol. 57, no. 5, pp. 1155–1168, 2009.
[23] X. Tong, F. Wu, and L. Qi, "Worst-case CVaR based portfolio optimization models with applications to scenario planning," *Optim. Methods Softw.*, vol. 24, no. 6, pp. 933–958, 2009.
[24] S. Han, S. Han, and K. Sezaki, "Development of an optimal vehicle-to-grid aggregator for frequency regulation," *IEEE Trans. Smart Grid*, vol. 1, no. 1, pp. 65–72, Jun. 2010.
[25] M. R. Sarker, Y. Dvorkin, and M. A. Ortega-Vazquez, "Optimal participation of an electric vehicle aggregator in day-ahead energy and reserve markets," *IEEE Trans. Power Syst.*, vol. 31, no. 5, pp. 3506–3515, Sep. 2016.
[26] K. Bruninx, H. Pandžić, H. Le Cadre, and E. Delarue, "On the interaction between aggregators, electricity markets and residential demand response providers," *IEEE Trans. Power Syst.*, vol. 35, no. 2, pp. 840–853, Mar. 2020.
[27] Schneider, Electric. "Microgrid energy management benchmark." [Online]. Available: https://data.exchange.se.com/explore/dataset/microgrid-energy-management-benchmark-metadata/information/ (Accessed: Jan. 6, 2020).
[28] J. Huang, B. Cui, X. Zhou, and A. Bernstein, "A generalized lindist-flow model for power flow analysis," 2021, *arXiv:2104.02118*.
[29] T. Hong, P. Pinson, S. Fan, H. Zareipour, A. Troccoli, and R. J. Hyndman, "Probabilistic energy forecasting: Global energy forecasting competition 2014 and beyond," *Int. J. Forecasting*, vol. 32, no. 3, pp. 896–913, 2016.
[30] A. Sardá-Espinosa, "Time-series clustering in R using the dtwclust package," *R J.*, vol. 11, no. 1, p. 22, 2019.
[31] A. Sardá-Espinosa, "Comparing time-series clustering algorithms in R using the dtwclust package," *R Package Vignette*, vol. 12, p. 41, Jan. 2017.
[32] A. Nemirovski and A. Shapiro, "Convex approximations of chance constrained programs," *SIAM J. Optim.*, vol. 17, no. 4, pp. 969–996, 2007.
[33] R. T. Rockafellar and S. Uryasev, "Conditional value-at-risk for general loss distributions," *J. Bank. Finance*, vol. 26, no. 7, pp. 1443–1471, 2002.
[34] N. Good, E. Karangelos, A. Navarro-Espinosa, and P. Mancarella, "Optimization under uncertainty of thermal storage-based flexible demand response with quantification of residential users' discomfort," *IEEE Trans. Smart Grid*, vol. 6, no. 5, pp. 2333–2342, Feb. 2015.
[35] S. Sarykalin, G. Serraino, and S. Uryasev, "Value-at-risk vs. conditional value-at-risk in risk management and optimization," in *State-of-the-Art Decision-Making Tools in the Information-Intensive Age*. London, U.K.: Informs, 2008, pp. 270–294.
[36] Elia NV. "Grid data." 2020. [Online]. Available: http://www.elia.be/en/grid-data

Mihaly Dolanyi received the bachelor's degree in mechanical engineering from the Budapest University of Technology and Economics. He completed the ENTECH Master Programme of InnoEnergy while studying with the Institut polytechnique de Grenoble, France, and the Karlsruhe Institute of Technology, Germany. He is currently pursuing the Ph.D. degree with the Energy Systems and Integration Research Group, KU Leuven, Belgium. His research concerns the game-theoretic modeling of energy markets.

Kenneth Bruninx (Member, IEEE) received the M.Sc. degree in energy engineering, the M.Sc. degree in management, and the Ph.D. degree in mechanical engineering from the University of Leuven (KU Leuven), Belgium, in 2011, 2015, and 2016, respectively. He is currently working as an Assistant Professor with the Faculty of Technology, Policy and Management, TU Delft, The Netherlands, and as a Research Fellow with the University of Leuven Energy Institute, TME Branch (Energy Conversion), Belgium.

Jean-François Toubeau received the degree in civil electrical engineering and the Ph.D. degree in electrical engineering from the University of Mons, Belgium, in 2013 and 2018, respectively, where he is currently a Postdoctoral Researcher with the Belgian Fund for Research (F.R.S/FNRS), Power Systems and Markets Research Group. His research mainly focuses on bridging the gap between machine learning and decision making in modern power systems.

Erik Delarue (Member, IEEE) received the M.S. degree in mechanical engineering and the Ph.D. degree in mechanical engineering from the University of Leuven (KU Leuven), Leuven, Belgium, in 2005 and 2009, respectively. He is currently an Associate Professor with the Department of Mechanical Engineering, University of Leuven, TME Branch (Energy Conversion) and active in EnergyVille.